Available online at www.sciencedirect.com
ScienceDirect
Journal of Catalysis 243 (2006) 278–291
JOURNAL OF CATALYSIS
www.elsevier.com/locate/jcat

Selective *ortho*-methylation of phenol with methanol over copper manganese mixed-oxide spinel catalysts

A. Satyanarayana Reddy, Chinnakonda S. Gopinath, Satyanarayana Chilukuri *

Catalysis Division, National Chemical Laboratory, Dr. Homi Bhabha Road, Pune 411008, India

Received 3 May 2006; revised 12 July 2006; accepted 13 July 2006

Available online 11 September 2006

Abstract

Methylation of phenol with methanol as an alkylating agent to produce 2,6-xylenol was investigated over copper manganese mixed oxide spinels, $Cu_xMn_{3-x}O_4$ ($x = 0$, 0.25, 0.5, 0.75, and 1) prepared through co-precipitation. The catalytic activity strongly depends on the composition, acid–base properties, and structural stability. Various parameters, including catalyst composition, reaction temperature, feed composition, and durability of the catalyst during methylation, were investigated. Mainly *o*-cresol and 2,6-xylenol, along with small amounts of mesitol, were found in the product. A high ortho-selectivity of 100%, with 2,6-xylenol selectivity of 74%, was observed over $Cu_{0.25}Mn_{2.75}O_4$ at 673 K. These catalysts were investigated using various techniques, including BET surface area, XRD, DRS UV–vis, TPD of NH_3 and CO_2, TPR, and X-ray photoemission spectroscopy (XPS). Powder XRD of the catalysts revealed the formation of copper–manganese spinels with hausmannite (Mn_3O_4) tetragonal structure, for $x = 0$–0.5, whereas an increase in copper content ($x > 0.5$) led to the formation of cubic $Cu_{1.5}Mn_{1.5}O_4$ phase. DRS UV–vis, and FTIR further supported the changes in structural phases observed by XRD. Temperature-programmed desorption of CO_2 and NH_3 showed that the catalysts have strong basicity along with weak acidity when $x = 0$ and 0.25. XPS and XAES analysis revealed the presence of only Cu^{2+} ions in fresh sample with $x = 0.25$, whereas for $x = 1.0$, both Cu^{1+} and Cu^{2+} were observed. The deactivation of the catalysts is attributed to structural changes occurring during the reaction. Catalytic activity is correlated with structure, as well as with acid–base properties.

Keywords: Phenol methylation; Ortho-alkylation; 2,6-Xylenol; Spinels; Copper–manganese oxides; Acidity–basicity

1. Introduction

Catalytic alkylation of phenols has received increased attention owing to the importance of alkyl phenols as starting materials for various commercial applications, including manufacture of dyes, antiseptics, drugs, insecticides, antioxidants, specialty paints, and plastics. Among alkyl phenols, *o*-cresol and 2,6-xylenol are the most sought after for the manufacture of agrochemicals, specialty plastics, and polymers. Ortho-cresol has applications in the synthesis of herbicides, whereas 2,6-xylenol is used in the manufacture of polyphenylene oxide (PPO) and special-grade paints [1,2]. Hence, there is a need to develop catalysts that produce these ortho-methyl phenols with high selectivity. Phenol alkylation reactions are usually carried out in the liquid phase using such catalysts as $AlCl_3$, BF_3, $TiCl_4$, H_2SO_4, HF, and others. All of these catalysts are beset with problems, including toxicity, corrosiveness, and difficulties with recycling and effluent disposal. Methylation of phenol can be carried out with methanol as an alkylating agent, either in the liquid phase using γ-Al_2O_3 [3] or in the vapor phase using supported vanadium–iron oxides [4]. However, the latter process requires very high temperatures, whereas both processes yield mixtures of methylated phenols.

Previous studies on methylation of phenol revealed the importance of acid–base properties of a catalyst on its activity and selectivity to the desired product [5,6]. Preparation of O- and C-alkylated phenols usually depends on reaction conditions, the nature of the catalyst, and surface acid–base properties [7–9]. A wide spectrum of catalysts have been reported for the vapor-phase alkylation of phenol, including single metal oxides, such as Mn_3O_4, CeO_2, Fe_2O_3, and MgO (with or without promoters) [10–13]; mixed metal oxides [14–18]; hydrotalcites [6,19]; zeolites [20–22]; Nafion-H and phosphoric acid [23]; sulfated

* Corresponding author. Fax: +91 20 2590 2633.
E-mail address: sv.chilukuri@ncl.res.in (S. Chilukuri).

0021-9517/$ – see front matter
doi:10.1016/j.jcat.2006.07.014

zirconia; and SO_3-HMS [24]. Tanabe et al. reported that catalysts with high acidity are very active but not so selective for ortho-alkylation [25], whereas, oxide catalysts that are basic in nature offer better selectivity for ortho-methyl phenols, particularly 2,6-xylenol. However, there is still ambiguity in correlation of acidity and/or basicity of the catalyst with C or O selectivity. It is difficult to come to a conclusion, based on literature reports, as to whether acidity or basicity (or both) is responsible for the selective production of 2,6-xylenol. It is generally accepted that metal oxide catalysts offer better selectivity for the formation of 2,6-xylenol than acidic zeolites. Attempts have been made to tailor catalysts by modifying acidity/basicity to achieve a desired product selectivity. Surface acid–base properties of mixed oxides containing MgO, Al_2O_3, and TiO_2 in various proportions have been investigated for methylation of phenol [7,9,15,16]. Most of the reports concur on the mechanism of C-alkylation on oxide catalysts, which involves formation of a π-complex with phenol on the Lewis acid sites while the adjacent basic sites adsorb the hydroxyl proton of the phenol [26].

Ferrite spinels with incorporation of different metals have been found to be active catalysts for C-alkylation of homo and heterocyclic aromatic compounds [26–32]. The commercial catalysts used presently for methylation of phenol are based mainly on magnesium oxide and vanadium–iron mixed oxides modified with promoters. However, they suffer from low intrinsic activity and rapid deactivation [33]. Spinels were found to be highly suitable for preparation of ortho-substituted methyl phenols [27]. Spinels have the composition AB_2O_4, where A- and B-cations occupy tetrahedral and octahedral sites, respectively. Physicochemical properties of spinels depend mainly on the nature of cations, the charge, and the distribution in tetrahedral/octahedral sites. Spinels demonstrate very interesting structural, electrical, and magnetic properties. Such properties as enhanced red–ox behavior make manganese-based oxides highly suitable for various catalytic reactions (i.e., hydrogenation of CO, oxidation of CO, selective catalytic oxidation) [34–37]. Mixed metal oxides are believed to exhibit better catalytic activity over individual oxides; therefore, many industrial processes use mixed oxides to prevent coke formation as well as to achieve better on-stream stability. Copper–manganese oxide spinels have been reported as catalysts for the decomposition of certain volatile organic compounds [38–41]. Cation distribution in a spinel influences its acid–base properties. Consequently, the present study attempts to unravel the effects on substitution of copper into manganese oxide (Mn_3O_4) spinel and its role in the methylation of phenol.

Most reports on alkylation of phenol using reducible metal oxides have correlated the catalytic activity with acid–base properties and have neglected the red–ox properties and/or structural changes, despite the fact that the catalysts can undergo irreversible reduction under reaction conditions. Hydrogen or CO evolved during the reaction as a result of partial oxidation or reformation with the help of H_2O produced during the reaction may lead to the reduction of metal oxide. An attempt has been made in this study to exploit red–ox properties in an effort to overcome catalyst deactivation as a result of reduction. To the best of our knowledge, acid–base properties of these systems have not been systematically explored with varying Cu and Mn concentrations. The present investigation correlates structural, red–ox, and acid–base properties of copper manganese oxide catalysts with their performance in the phenol methylation reaction.

2. Experimental

2.1. Preparation of copper–manganese oxides

A series of copper–manganese mixed oxides, $Cu_xMn_{3-x}O_4$ with $x = 0.25$, 0.5, 0.75, and 1.0, were prepared through co-precipitation with KOH using dilute acetate solutions of Cu and Mn. In a typical synthesis for the preparation of 7 g of $Cu_xMn_{3-x}O_4$ with $x = 0.25$, stoichiometric amounts of premixed solutions (0.1 M) of Mn and Cu acetates (20.40 and 1.52 g) were precipitated using a 0.25 M KOH solution. Both alkali and salt solutions were added simultaneously, under vigorous stirring at 353 K. The final pH of the gel was adjusted to 10.5 and aged at 353 K for 12 h. The precipitate thus obtained was filtered and washed thoroughly with demineralized water until the pH of the filtrate was ∼7.5. The sample was dried at 383 K for about 12 h and calcined at 773 K in air. The chemical analysis of the oxide samples was carried out using atomic absorption spectroscopy (AAS). The samples are designated herein as CM_x, where x denotes the fraction of copper taken for the preparation of $Cu_xMn_{3-x}O_4$.

2.2. Characterization methods

The BET surface area (S_{BET}) of the samples was measured by nitrogen sorption at 77 K using a NOVA-1200 unit. The catalyst samples were evacuated at 573 K for 3 h before N_2 adsorption. Powder X-ray diffraction (XRD) data were obtained on a Rigaku X-ray diffractometer (model DMAX IIIVC) equipped with a Ni-filtered Cu$K\alpha$ ($\lambda = 0.1541$ nm, 40 kV A, 30 mA) radiation and graphite crystal monochromator. The data was collected in the 2θ range of 20°–90° with a step size of 0.02° and a scan rate of 0.5° min^{-1}. XRD of spent catalyst was also recorded after subjection to 4 h of phenol methylation at 673 K. The mean crystallite size of the samples was calculated using the Debye–Scherrer equation [42], using the FWHM value corresponding to high intense peak at 36° and 40.54° for fresh and spent catalysts, respectively. Unit cell parameters were determined using PDP11 software.

Diffuse-reflectance UV–visible spectra were recorded on a Shimadzu UV-2550 spectrophotometer in diffuse reflectance mode in the 200–800 nm range, at room temperature. FTIR spectra of the samples were recorded on a Shimadzu 8300 FTIR at ambient conditions. The spectra were recorded using thin circular discs made by pressing a mixture of catalyst with KBr.

Temperature-programmed desorption (TPD) of CO_2 and NH_3 were carried out using a Micromeritics Autochem model 2910 instrument. Fresh calcined samples (∼300 mg) were pretreated in helium at 773 K before adsorption of the probe molecules (10% CO_2 or 10% NH_3 in helium). During desorption,

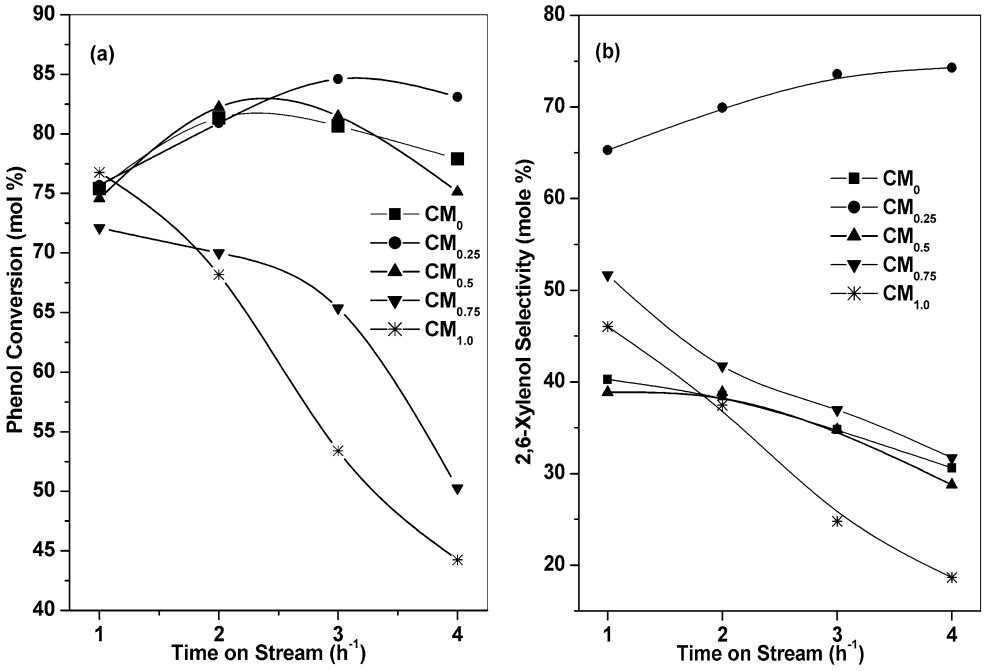

Fig. 1. Effect of catalyst composition on phenol conversion (a) and 2,6-xylenol selectivity (b) on copper–manganese spinel catalysts at 673 K. Methanol to phenol molar ratio 5, WHSV 1 h^{-1}.

the sample was heated in helium flow (40 ml/min) at a ramp of 10 K/min. The amount of CO_2/NH_3 desorbed from the sample was estimated from the area under the peak after taking the thermal conductivity detector response into consideration. Temperature-programmed reduction (TPR) profiles were also obtained using the same instrument. The samples were pretreated in high-purity (99.98%) argon (20 ml/min) at 773 K for 3 h. After cooling to ambient, argon was replaced with a 5% H_2 in argon mixture, and the catalyst was heated up to 873 K at a heating rate of 5 K/min. The flow rate of H_2–Ar mixture used for this purpose was 40 ml/min. The water produced during the reduction step was condensed and collected in a cold trap immersed in the slurry of isopropanol–liquid nitrogen mixture.

X-ray photoemission spectra (XPS) were acquired on a VG Microtech Multilab ESCA 3000 spectrometer using a non-monochromatized Mg$K\alpha$ X-ray source ($h\nu = 1253.6$ eV). Disks of fresh sample were scraped in situ before the spectra were recorded. Selected spectra were also recorded with Al$K\alpha$ X-ray ($h\nu = 1486.6$ eV) source to eliminate the overlap between different Auger and core levels. Details on the instrument and XPS measurements have been reported previously [27].

2.3. Catalytic activity studies

Catalysts were evaluated in a vertical downflow, fixed-bed glass reactor placed in a two-zone split furnace (Geomechanique, France). The reaction data were collected at atmospheric pressure in the temperature range 623–723 K, using 2 g of catalyst with a particle size of 10–20 mesh. The temperature of the catalyst bed was continuously monitored by a Cr–Al thermocouple. Before the reaction, catalysts were activated in flowing dry air at 773 K, followed by cooling to the reaction temperature in nitrogen atmosphere. The reactant mixture was fed to the reactor using a high-precision syringe pump (ISCO Model 500D), at a flow rate corresponding to WHSV $= 1\ h^{-1}$. The reactant mixture was evaporated and preheated to the reaction temperature in the upper part of the reactor before it entered the catalyst bed. The product mixture was cooled using a chilled water condenser and collected in a separator. Analysis of the product mixture was carried out at regular intervals using a gas chromatograph (HP 6890N) equipped with BP-5 capillary column (50 m, 0.32 mm i.d., 1 μ film thickness) and a FID. All of the products were identified using pure authentic (Aldrich) standards. Conversion of phenol was calculated based on the fraction of phenol reacted, whereas the selectivity was obtained based on the percentage of the given alkyl phenol in the products.

3. Results

3.1. Catalytic activity

Fig. 1 shows the phenol conversion and 2,6-xylenol selectivity with time on stream (TOS) on copper–manganese oxide catalysts at 673 K. The screening of catalysts was carried out under identical conditions using a methanol-to-phenol ratio of 5 at a space velocity of 1 h^{-1}. Phenol alkylation yielded mainly ortho-methylated products of *o*-cresol and 2,6-xylenol, with a small amount (<2%) of mesitol. Phenol conversion and *o*-cresol/2,6-xylenol selectivity varied significantly with TOS depending on the catalyst composition. The phenol conversion was comparable (around 75%) on all of the catalysts up to 1 h TOS. Nonetheless, phenol conversion decreased more rapidly at TOS $\geqslant 3$ h on high copper-containing catalysts ($CM_{0.75}$ and $CM_{1.0}$), than on the other compositions. The differences in activity were more apparent after 2 h TOS, particularly for samples with $x \geqslant 0.5$.

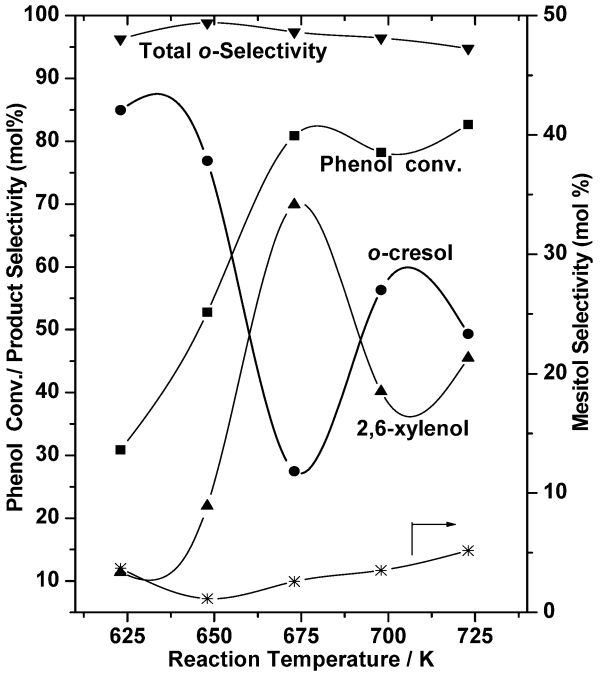

Fig. 2. Influence of reaction temperature on phenol conversion and product selectivity for $CM_{0.25}$ catalyst. Methanol to phenol molar ratio 5, WHSV 1 h^{-1}, TOS-2 h.

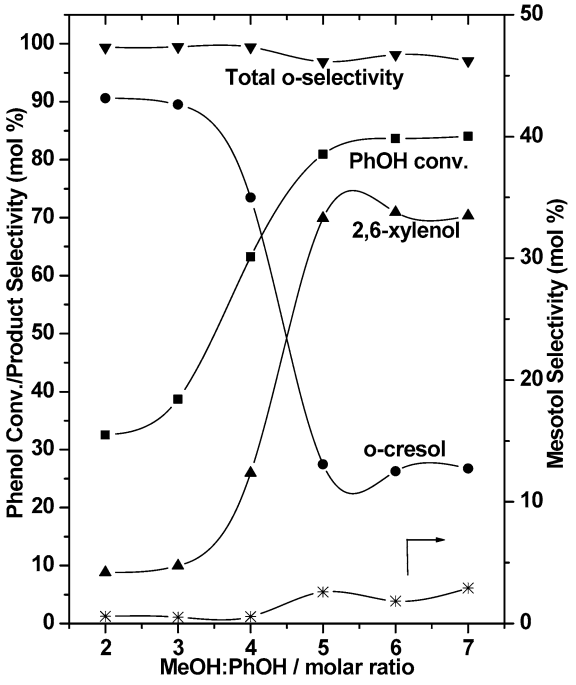

Fig. 3. Effect of methanol to phenol mole ratio on phenol conversion and product selectivity. Catalyst $CM_{0.25}$ ($Cu_{0.25}Mn_{2.75}O_4$), WHSV 1 h^{-1}, $T = 673$ K, TOS-2 h.

A clear trend was observed in the deactivation of catalysts, which deactivated more rapidly with increasing copper content. The catalyst with $x = 0.25$ showed good activity and the highest 2,6-xylenol selectivity. The catalysts with increasing copper content either deactivated rapidly or showed lower selectivity to 2,6-xylenol. Pure manganese oxide catalyst that we prepared was more active at lower temperatures than the reported catalyst prepared from carbonate precursors [10]. The 2,6-xylenol selectivity fell continuously for catalysts with $x > 0.25$, even though the initial selectivities were higher. The $CM_{0.25}$ sample demonstrated good activity as well as 2,6-xylenol selectivity, with hardly any deactivation, for the duration of the experiment.

Fig. 2 shows variation of phenol conversion and selectivity to various ortho-alkyl phenols as a function of temperature (623–723 K) on $CM_{0.25}$ catalyst, using feed with a phenol-to-methanol molar ratio of 1:5. The conversion of phenol increased with temperature, reaching a maximum at 673 K. It remained nearly the same thereafter with further increases in reaction temperature. Similarly, the yield of 2,6-xylenol reached a maximum at 673 K. The concentration of *o*-cresol was very high at lower temperatures and decreased with increasing reaction temperature, with a concomitant increase in 2,6-xylenol content. This clearly shows that the mono-methylation was predominant at lower temperatures, whereas 2,6-xylenol selectivity increased at higher temperatures as a result of consecutive reactions at the expense of *o*-cresol. Mesitol concentration also increased with temperature, and methanol conversion increased from about 50 to 60% with increasing temperature. At the same time, no aliphatic compounds were observed in the product.

Alkylation of phenol was carried out using various molar ratios of phenol to methanol over $CM_{0.25}$ at 673 K. The data on conversion of phenol and selectivity to various ortho-alkylphenols are given in Fig. 3. As could be expected, phenol conversion increased linearly with increasing methanol concentration in the feed, reaching close to maximum at a phenol-to-methanol ratio of 1:5. Only a small increase in conversion resulted from a further increase in methanol content in the feed. Surprisingly, 2,6-xylenol selectivity also followed a simi-

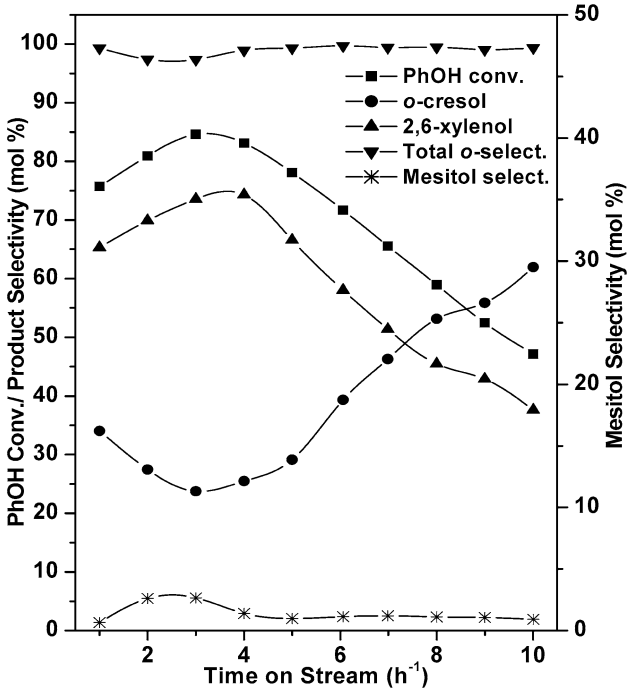

Fig. 4. Time on stream behavior of $CM_{0.25}$ catalyst ($Cu_{0.25}Mn_{2.75}O_4$) during phenol methylation reaction. $T = 673$ K, methanol to phenol mole ratio of 5, WHSV 1 h^{-1}.

lar trend, whereas it remained constant for feed ratios above 5. At lower methanol-to-phenol ratios, *o*-cresol was the major product. As noted earlier, opposite trends were observed for *o*-cresol and 2,6-xylenol selectivity [27]. In fact, concentration of *o*-cresol in the product fell to ∼24 mol% from the 90 mol% observed for a methanol-to-phenol molar ratio of 2. Mesitol, which is expected as a result of consecutive alkylation of dimethyl phenols, increased monotonously with the molar ratio. Because 2,6-xylenol selectivity was greatest at a molar ratio of 5, further studies were carried out using this ratio.

Fig. 4 presents TOS trend of phenol methylation on the $CM_{0.25}$ catalyst. Constant phenol conversion around 80 mol% was observed up to 4–5 h, with conversion decreasing continuously with time thereafter. Although the total ortho-selectivity remained the same, 2,6-xylenol selectivity decreased with a simultaneous increase in *o*-cresol content in the product. As a result, mesitol concentration also decreased to negligible levels. We address the reasons for this catalyst deactivation later in the paper.

3.2. Catalyst characterization

The physicochemical properties of fresh and spent catalysts (after TOS = 4 h, $T = 673$ K, MeOH: PhOH = 5:1) are summarized in Table 1. The metal contents obtained from bulk chemical analysis (AAS) are in good agreement with the input metal concentrations (given in parentheses) used for preparation. Although BET surface area of the catalysts does not follow any particular trend, catalysts with high copper content in general have a relatively high surface area. Surface area of the spent catalysts (given in parentheses) decreased after phenol methylation reaction; however, surface areas of CM_0 and $CM_{0.25}$, which were relatively low to begin with, did not change significantly after the reaction. Crystallites sizes of the fresh and spent catalysts (given in parentheses) are also summarized in Table 1. The crystallite size, in the range 14–20 nm, increased after methylation for all fresh samples except $CM_{0.25}$. This increase was greater for the samples with high copper content.

XRD patterns of fresh and spent catalysts are shown in Fig. 5. The sample without copper (CM_0) showed a hausmannite (Mn_3O_4) structure (JCPDS file No. 24-734) after calcination at 773 K. A small amount of Mn_5O_8 (JCPDS file No. 39-1218) was also found in all fresh calcined samples. The diffraction lines at 2θ values of 21.6, 47.8, and 66.2 are assigned to Mn_5O_8. In addition to Mn_5O_8, a small amount of Mn_2O_3 (peak at 33.01°, JCPDS file No. 10-0069) was also found in samples with low copper content. The hausmannite structure did not undergo any change after incorporation of small amounts of copper ($CM_{0.25}$), whereas at increasing copper content ($CM_{0.75}$ and $CM_{1.0}$), it transformed to another spinel phase. The powder XRD patterns obtained for these samples have been assigned to $Cu_{1.5}Mn_{1.5}O_4$ spinel (JCPDS file No. 35-1171). A gradual transformation from hausmannite to $Cu_{1.5}Mn_{1.5}O_4$ phase was observed with increasing copper concentration, finally yielding $Cu_{1.5}Mn_{1.5}O_4$ for the highest copper content ($x = 1.0$) used in this study. The absence of copper oxide in all samples may point to the substitution of copper into the manganese oxide lattice, leading to a solid solution of copper–manganese oxide as a major phase. A clear shift toward lower 2θ values was observed for the peak at ∼36, which is shown as an inset. Cell parameters, calculated using PDP11 software, show a gradual transformation of tetragonal spinel to cubic (i.e., a decrease in "c" value and an increase in "a" value) with increasing copper content. The respective values are $a = 5.73$ and $c = 9.41$ Å for CM_0, $a = 5.74$ and $c = 9.40$ Å for $CM_{0.25}$, and $a = 5.75$ and $c = 9.38$ Å for $CM_{0.5}$. In comparison, the cubic phases of $CM_{0.75}$ and $CM_{1.0}$ samples have values of $a = 8.26$ and 8.28 Å, respectively. XRD of spent catalysts analyzed after 4 h

Table 1
Catalyst composition, crystallites size, crystalline phase, and BET surface area values of copper–manganese oxide $Cu_xMn_{3-x}O_4$ catalysts

Catalyst	Metal concentration (wt%)[a]		Crystallite size (nm)	Crystallite phases	S_{BET} (m^2/g)
	Mn	Cu			
CM_0	66.40 (72.05)[b]	–	20.92 (20.83)[c]	Mn_3O_4[d], Mn_5O_8	21 (20)[c]
$CM_{0.25}$	55.85 (64.43)	6.00 (6.87)[b]	14.04 (15.23)	Mn_3O_4, Mn_5O_8, Mn_2O_3	17 (16)
$CM_{0.5}$	57.03 (58.94)	12.26 (13.61)	18.59 (25.73)	Mn_3O_4, Mn_5O_8, Mn_2O_3	36 (25)
$CM_{0.75}$	52.98 (52.57)	18.78 (20.24)	16.74 (22.24)	$Cu_{1.5}Mn_{1.5}O_4$, Mn_5O_8	44 (28)
$CM_{1.0}$	23.75 (26.74)	23.00 (26.74)	15.97 (38.25)	$Cu_{1.5}Mn_{1.5}O_4$, Mn_5O_8	33 (22)

[a] Chemical analysis values are obtained from AAS.
[b] Numbers in brackets are expected values.
[c] Values from used catalysts.
[d] Hausmannite.

Table 2
Surface acidity and basicity of copper–manganese oxides derived from TPD

Catalyst	CO_2 desorption temperature (K)	CO_2 desorbed (mmol)	Total CO_2 desorbed (mmol)	NH_3 desorption temperature (K)	NH_3 desorbed (mmol)	Total NH_3 desorbed (mmol)
CM_0	434, 523	3.39, 2.75	7.04	433, 502, 597	71.37, 39.61	111
$CM_{0.25}$	434, 521	7.86, 8.99	18.96	427, 497, 589	95.42, 35.56	131
$CM_{0.5}$	428, 500	5.69, 11.03	17.44	423, 481, 552	68.72, 54.59	152
$CM_{0.75}$	415, 456	3.35, 9.2	23.4	418, 476, 555	68.72, 54.59	186
$CM_{1.0}$	406, 442	5.33, 6.46	22.45	–	–	198

of phenol methylation at 673 K, are given in Fig. 5b. All of the samples underwent reduction during the reaction, yielding MnO (JCPDS file No. 7-0230) and metallic copper. Spent catalyst samples with high copper content ($x \geqslant 0.5$) showed XRD peaks at 2θ values 43.30° and 50.62°, which are characteristic of metallic copper (JCPDS file No. 4-0836).

Fig. 6 presents UV–visible absorption spectra obtained for copper–manganese oxide catalysts. The electronic spectra of CM_0 and $CM_{0.25}$ are mostly similar, showing absorption in the 200–600 nm region, in good agreement with the hausmannite structure [43]. Assigning this spectrum to individual absorption of metal ions is cumbersome. Because Mn_3O_4 is a normal spinel, the Mn^{2+} and Mn^{3+} cations would be expected to be in tetrahedral and octahedral sites, respectively. The charge transfer continuous bands reported at around 240–305 nm are assigned to $O^{2-} \rightarrow Mn^{2+}$ and $O^{2-} \rightarrow Mn^{3+}$ transitions, respectively [43], whereas the absorption band in the visible region attributed to single spin allowed d–d transition of Mn^{3+} in octahedral environment, which is expected at about 500 nm [43]. A clear change occurred in the DRS spectra after Cu incorporation, particularly for samples with $x \geqslant 0.5$, with distinct bands (~425 nm) in the visible region. These bands may be attributed to distorted d–d transitions originating from Mn^{3+} [43–47]. No bands in the region of 800 nm were observed that could be attributed to d–d transitions of Cu^{2+} in the octahedral environment [48,49].

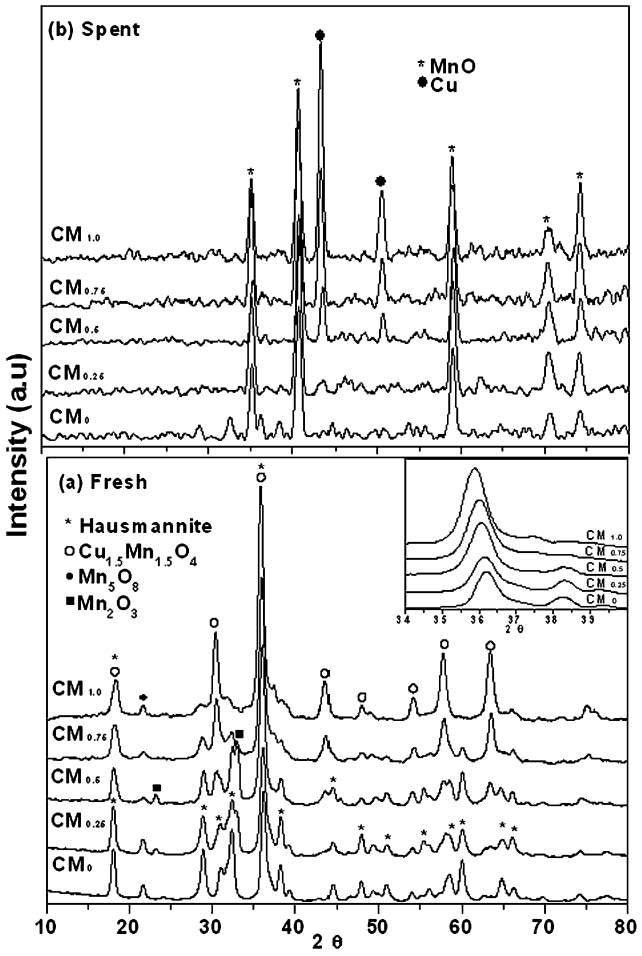

Fig. 5. X-ray diffraction pattern of (a) fresh and (b) spent copper–manganese spinel type catalysts.

FTIR spectra of fresh catalysts are shown in Fig. 7. Three bands were observed for samples with predominantly hausmannite structure (low-Cu samples) at 429, 516, and 628 cm^{-1}, in good agreement with the previous reports [43,46,47,50–52]. The IR spectrum of $CM_{0.25}$ is identical to that of CM_0. The effect of copper incorporation is especially evident for samples with $x \geqslant 0.5$. The first two bands at 429 and 516 cm^{-1} disappeared for samples with $x \geqslant 0.5$. Although the band at 628 cm^{-1} was still present for $CM_{0.5}$, it disappeared for $CM_{0.75}$ and $CM_{1.0}$. Hence, the IR results clearly show the transformation of hausmannite ($x \leqslant 0.25$) to $Cu_{1.5}Mn_{1.5}O_4$ phase with increasing Cu content.

TPR profiles of freshly calcined samples are given in Fig. 8. The sample CM_0 (i.e., Mn_3O_4) shows two reduction peaks with temperature maxima (T_{max}) at 565 and 705 K. These peaks may be assigned to the reduction of surface and bulk Mn^{3+}, respectively, to Mn^{2+}. A clear decrease in reduction temperature was observed after incorporation of copper. In addition, a broad low-temperature reduction peak at about 440 K was observed for all copper-containing catalysts. The intensity of this peak was found to increase with increasing copper content. The T_{max} of the main reduction peak was higher than the T_{max} observed for pure CuO (~500 K), but lower than that of bulk Mn_3O_4 (~700 K). The powder XRD pattern obtained after TPR experiment revealed the formation of MnO and Cu. Further reduction

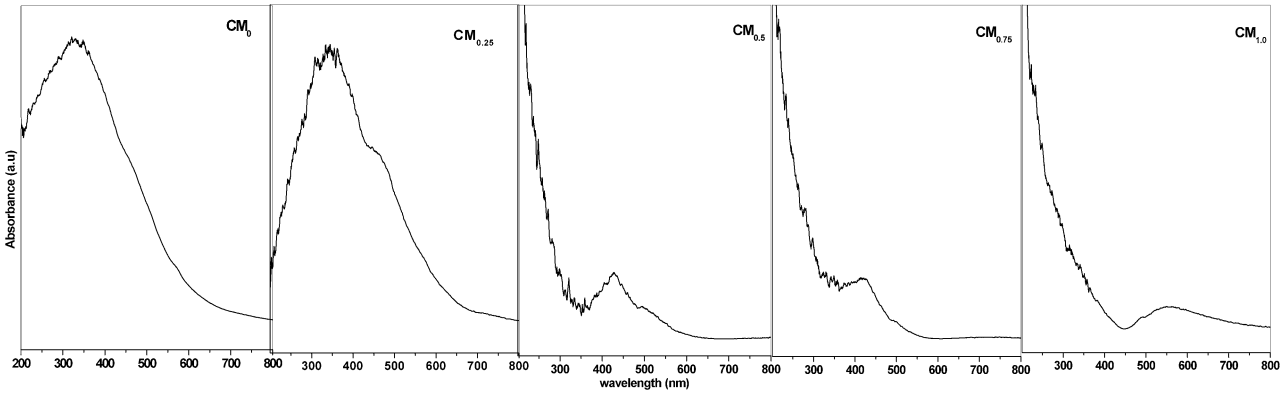

Fig. 6. UV–vis spectra of calcined copper–manganese oxide catalysts, $Cu_xMn_{3-x}O_4$ as a function of copper content.

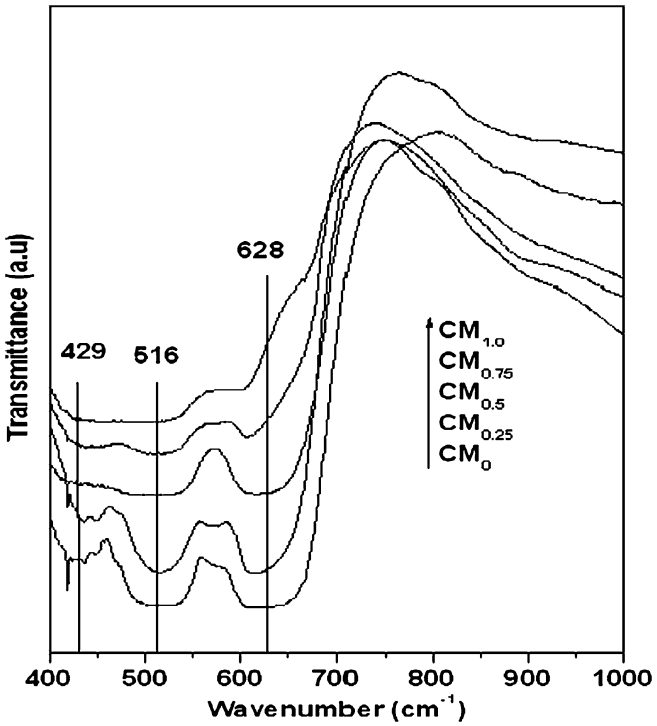

Fig. 7. FTIR spectra of calcined $Cu_xMn_{3-x}O_4$ catalysts.

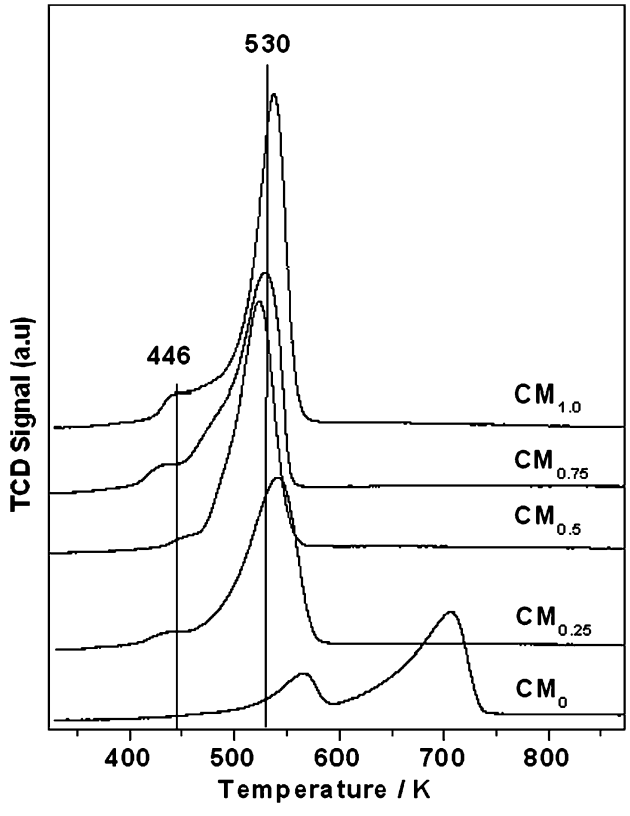

Fig. 8. TPR profiles of calcined copper–manganese oxide catalysts as a function of copper content.

of Mn^{2+} is not thermodynamically feasible under the experimental conditions. The reduction in peak width (FWHM) for the high copper-containing samples ($x \geqslant 0.5$) demonstrates that

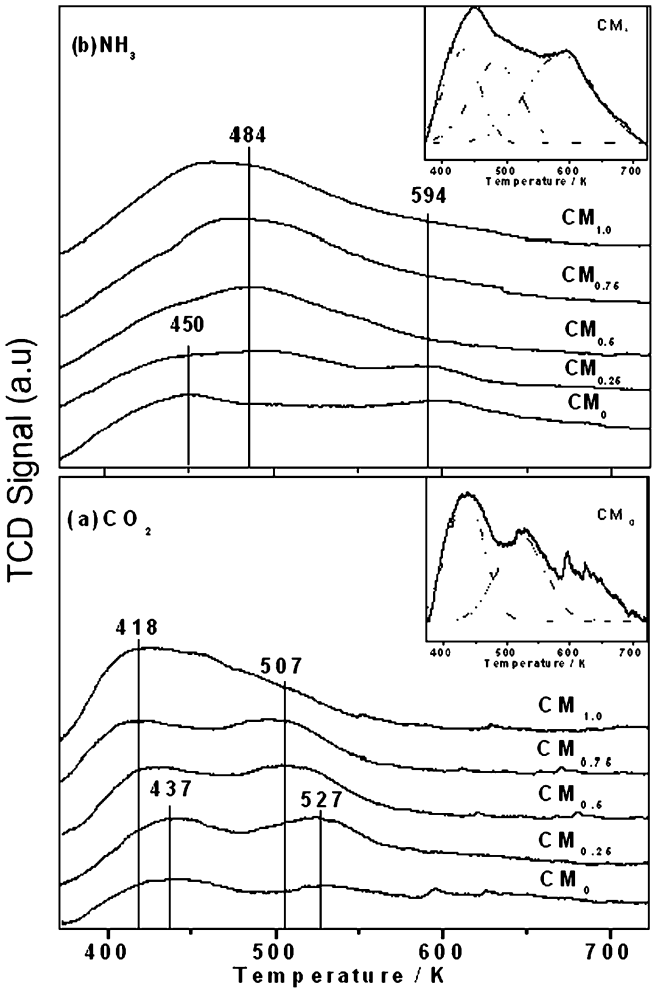

Fig. 9. Temperature programmed desorption profiles of (a) CO_2 and (b) NH_3 on copper–manganese oxide catalysts.

reduction of Cu^{2+} promoted the reducibility of Mn^{3+}. The peak maxima (T_{max}) of the samples shifted to lower temperatures initially up to a copper content of $x = 0.5$, and thereafter increased marginally to higher temperatures for samples with $x > 0.5$. This temperature shift may be attributed to the change of the phase, as observed by XRD.

Fig. 9 shows the results of TPD studies of CO_2 and NH_3 for fresh catalysts. The TPD of probe molecules such as NH_3 and pyridine are widely used for acidity characterization, whereas CO_2 is ideal for probing basicity of oxides. TPD of CO_2 shows that desorption occurred below 573 K, with peaks centered at around 437 and 527 K for CM_0 and $CM_{0.25}$ catalysts. This shows that there are two kinds of sorption sites for CO_2 on the surface of these catalysts, which may be attributed to weak and moderately strong basic sites. For catalysts with higher copper content ($x \geqslant 0.5$), a shift of the desorption peak toward lower temperatures was observed, demonstrating that basic sites in CM_0 and $CM_{0.25}$ have relatively higher strength. TPD of NH_3 on these catalysts is shown in Fig. 9b. These catalysts, particularly CM_0 and $CM_{0.25}$, exhibited three temperature maxima at 450, 484, and 594 K, demonstrating that they have acid sites of different strengths. Total acidity, obtained from desorbed NH_3, increased with increasing copper content (Table 2).

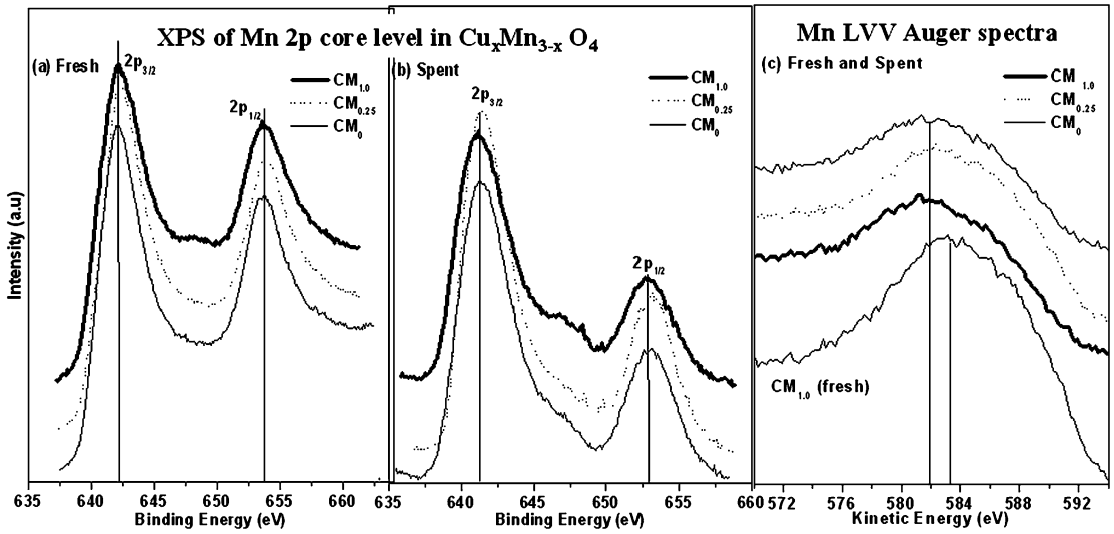

Fig. 10. Mn 2p photoemission spectra of (a) fresh, (b) spent and Mn LVV of fresh and spent $Cu_xMn_{3-x}O_4$ catalysts. Spent catalysts are obtained after 4 h of phenol methylation reaction at $T = 673$ K.

3.3. XPS analysis

Surface characterization of fresh and spent catalysts (CM_0, $CM_{0.25}$, and $CM_{1.0}$) was carried out by XPS and X-ray-initiated Auger electron spectroscopy (XAES).

3.3.1. Mn 2p core level and Mn-LVV Auger transition

Mn 2p photoemission spectra of fresh and spent catalysts along with Mn-LVV Auger transitions are shown in Fig. 10. A binding energy (BE) value of 642.1 ± 0.1 eV with ΔE of 11.4 ± 0.1 eV was observed for all of the catalysts, indicating that the oxidation state of Mn was 3+. These BEs observed for Mn $2p_{3/2}$ are in good agreement with those reported previously [53,54]. Hausmannite Mn_3O_4 has a spinel structure containing both Mn^{2+} and Mn^{3+} ions. Oku et al. reported that it is difficult to distinguish between the oxidation states of Mn in Mn_3O_4 using XPS [55]. Allen et al. reported that BE values of $2p_{3/2}$ peak for the manganese cations in MnO, Mn_3O_4, Mn_2O_3, and MnO_2 at 640.9, 641.7, 641.8, and 642.4, respectively [56]. Mn 2p peaks of spent catalysts were at 641.1, 641.4, and 641.4 eV for CM_0, $CM_{0.25}$ and $CM_{1.0}$, respectively. Mn-LVV Auger spectra of fresh $CM_{1.0}$ and spent CM_0, $CM_{0.25}$, and $CM_{1.0}$ catalysts are shown in Fig. 10c. Because the Mn-LVV spectra of fresh catalysts are similar, only the $CM_{1.0}$ spectrum is given in Fig. 10c, to demonstrate the changes from fresh to spent catalysts. A broad Auger transition can be seen between 576 and 592 eV for all of the samples. A shift in energy to lower (KE) for spent catalysts compared with fresh catalyst ($CM_{1.0}$) can be observed. The spectra from spent CM_0 and $CM_{0.25}$ are identical. The shift in the KE of fresh and spent $CM_{1.0}$ indicates the change in the oxidation state of Mn after phenol methylation.

3.3.2. Cu 2p core level

XPS spectra of Cu $2p_{3/2}$ core level for fresh and spent $CM_{0.25}$ and $CM_{1.0}$ catalysts are shown in Fig. 11. A main peak at 934.1 eV for the fresh catalysts with a satellite peak at around 942 eV was observed for both $CM_{0.25}$ and $CM_{1.0}$. Their FWHM values were found to be 2.6 and 3.3 eV, respectively. The BE of Cu $2p_{3/2}$ peak in CuO is reported to be about 933.6 eV [53,54], with a shake up satellite at 940–945 eV. The BE values of our samples are in good agreement with those reported previously. In the case of $CM_{1.0}$, an additional peak at lower BE (i.e., 931.0 eV) was seen along with the main peak at 934.1 eV. This peak indicates the presence of Cu^{1+}/Cu^0 species. The $2p_{3/2}$ peak of Cu^{1+} in Cu_2O is reported to be at 932.2 ± 0.3 eV [57]; for Mn-containing oxides, this would be expected at around 931 eV [58]. These experimental observations are in good agreement with the formation of Cu^{1+} and Mn^{4+} as a result of reduction–oxidation equilibrium $Cu^{2+} + Mn^{3+} \rightarrow Cu^{1+} + Mn^{4+}$, which is expected on copper substitution [58]. XPS of spent $CM_{0.25}$ catalysts gave a single peak for Cu 2p at 932.5 eV with a FWHM of 1.2 eV with no satellite peaks. Similarly, $CM_{1.0}$ showed only one peak, at 932 eV, with a FWHM of 1.4 eV. However, in this study, the main Cu 2p peak at 931.2 eV from $CM_{1.0}$ could be assigned to Cu^{1+}, which exhibited no satellite peak. However, metallic copper (Cu^0) also exhibited similar BE values as for Cu^{1+}, and hence making identification of oxidation states merely from the XPS of Cu 2p rather difficult.

3.3.3. Cu-$L_3M_{45}M_{45}$

Auger electron transition modifying Auger parameter α' distinguishes the different oxidation states of Cu in the same or related compounds [27,53]. The Cu-$L_3M_{45}M_{45}$ Auger spectra of fresh and spent catalysts are shown in Fig. 12. The $CM_{0.25}$ catalyst exhibited the Cu-$L_3M_{45}M_{45}$ line at a KE of 917.3 eV. A further increase in copper content of the sample shifted the peak to 917.7 eV. For pure CuO, this peak has been reported at 917.6 eV [27,53]. The values of α' determined for fresh $CM_{0.25}$ and $CM_{1.0}$ catalysts are 1851.4 and 1851.6, very close to the value observed for CuO (1851.5). The additional value of $\alpha' =$ 1848.7 eV obtained for $CM_{1.0}$ from the low-BE Cu $2p_{3/2}$ peak supports the presence of Cu^{1+}. In contrast to the fresh catalysts, a peak at a KE of 916.6 eV was observed for $CM_{0.25}$ spent cata-

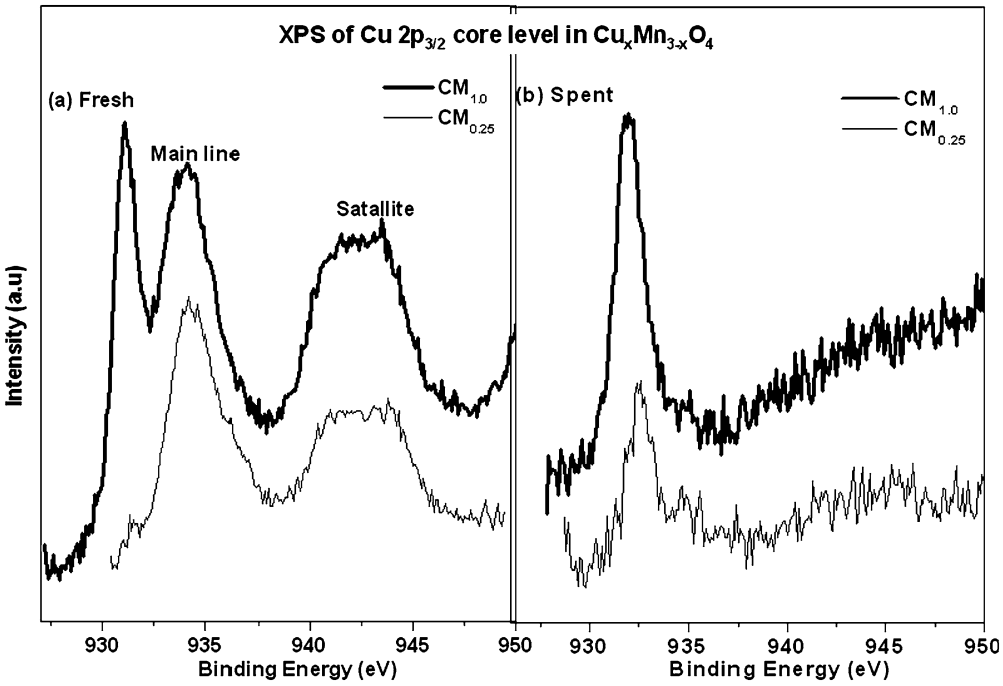

Fig. 11. Cu 2p core level XPS spectra of (a) fresh and (b) spent $Cu_xMn_{3-x}O_4$ catalysts.

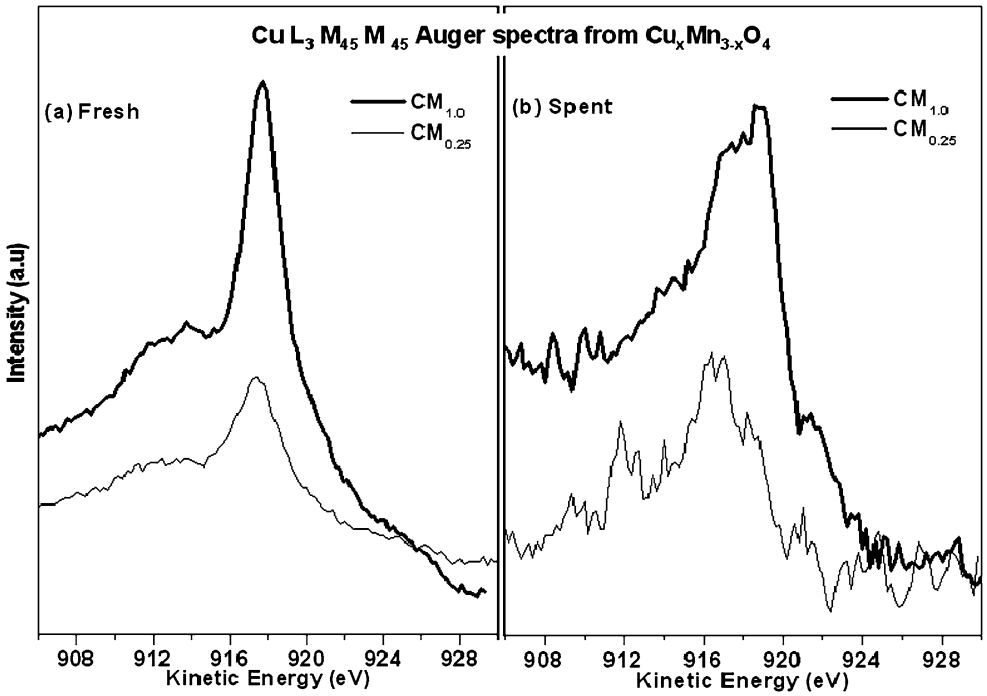

Fig. 12. X-ray initiated Augur electron spectra (XAES) from Cu-$M_3M_{45}M_{45}$. (a) Fresh and (b) spent $Cu_xMn_{3-x}O_4$ catalysts.

lyst, whereas a broad peak that can be resolved into two peaks at 916.7 and 918.8 eV was observed for $CM_{1.0}$. The KE values indicate the formation of Cu^{1+} for spent $CM_{0.25}$ catalyst, whereas both Cu^{1+} and Cu^0 were present in $CM_{1.0}$ spent catalyst. For spent catalysts, the α' values were 1849.1 eV for $CM_{0.25}$ and 1848.7 and 1850.8 eV for $CM_{1.0}$, further supporting the presence of Cu^{1+} in the former and both Cu^{1+} and Cu^0 in the latter. However, surface oxidation of Cu → Cu^{1+} when the spent catalysts were exposed to ambient atmosphere cannot be ruled out.

3.3.4. Valence band photoemission

XPS spectra of the valence band (VB) region obtained from fresh and spent catalysts are shown in Figs. 13a and 13b, respectively. The main VB observed below 9 eV had contributions from 3d orbitals of Cu and Mn. At the $h\nu = 1253.6$ used in these experiments, the photoionization cross-section (σ) value (Cu 3d = 0.021, Mn 3d = 0.0026, and O 2p =0.0005 Mb) [59] was the dominant factor determining the spectral intensity. The above data suggest that the contribution from O 2p was negli-

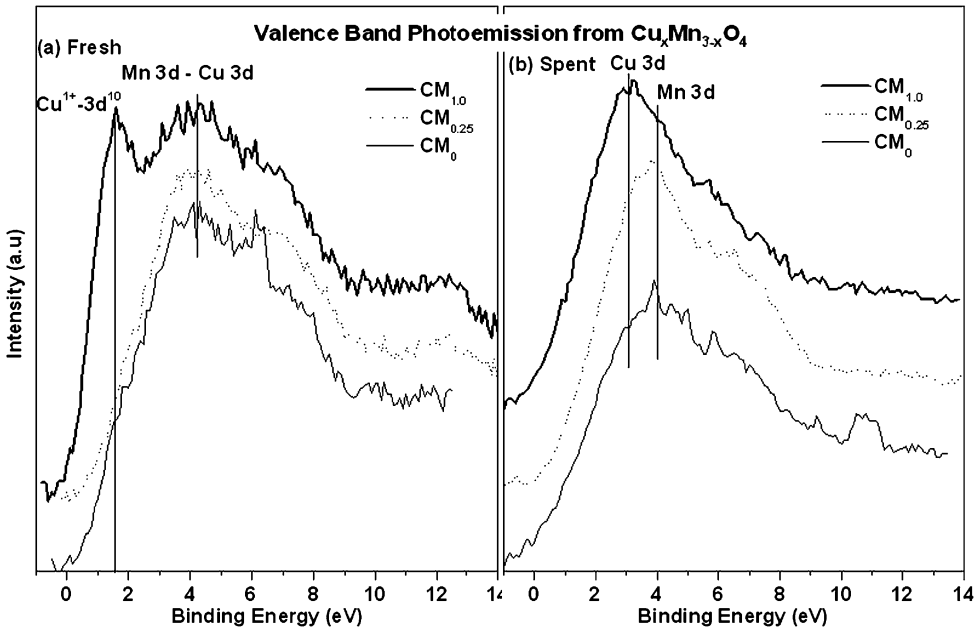

Fig. 13. Valence band XPS spectra of fresh and spent copper manganese oxide catalysts.

gible. Similarly, Cu 3d should make significant contributions to the VB. The VB assignments are straightforward based on the intensity and BE of the bands. The high-intensity VB observed on CM_0 at 4 eV is due to Mn 3d bands. The intensity of VB increased with increasing copper content along with a new peak at 2 eV and a satellite around 12 eV. This observation clearly suggests that the new features were from Cu 3d bands. The band at low BE (2 eV) can be attributed to a Cu-$3d^{10}$ band [27]. An overlap of Mn 3d and Cu 3d was observed at around 4 eV from fresh catalysts. The intensity variation observed with increasing copper content is due mostly to the high σ of the Cu 3d bands. The comparatively low-intensity features observed between 6 and 8 eV can be attributed to O 2p bands.

Dramatic changes observed on spent catalysts from core levels are reflected strongly in the VB spectra: (i) main VB shifting toward lower BE with increasing copper content; (ii) the satellite appearing at around 12 eV on fresh catalysts disappearing on $CM_{0.25}$ and $CM_{1.0}$, and (iii) the disappearing Cu^{1+}-$3d^{10}$ band on $CM_{1.0}$ due to reduction of $Cu^{1+} \rightarrow Cu$ and hence an associated shift in BE of the 3d bands. These observations clearly suggest increasing catalyst reduction from CM_0 to $CM_{1.0}$ Although the Cu 3d and Mn 3d energy bands overlapped, no interaction between Cu and MnO occurred, obviously due to reduction.

4. Discussion

Catalytic studies of phenol methylation over various Cu_x-$Mn_{3-x}O_4$ ($x = 0$–1) catalysts show that an optimum concentration of copper was required to obtain high 2,6-xylenol selectivity and that the catalyst $CM_{0.25}$, showed superior activity and selectivity. At lower reaction temperatures ($\leqslant$650 K), *o*-cresol selectivity was very high; however, *o*-cresol selectivity decreased with increasing temperature with a concomitant increase in 2,6-xylenol selectivity, whereas the maximum yield of 2,6-xylenol was obtained at 673 K. This clearly shows that mono-alkylation was dominant at lower temperatures and di-alkylation to 2,6-xylenol increased at higher temperatures, due mainly to consecutive methylation of *o*-cresol. This shows that the reaction temperature significantly influences the rate of consecutive methylation. The important observation is that the total ortho-selectivity remained almost the same (>95%) within the temperature range studied. However, a decrease in alkyl phenol content was observed at higher temperatures, which may be attributed to prevalence of dealkylation reactions. Among the minor products found was mesitol, the concentration of which also increased with increasing temperature. This increase could be due either to consecutive alkylation of product xylenol or to disproportionation of xylenols. A similar trend was observed when feeds containing various phenol-to-methanol ratios were used. The reduction in the concentration of *o*-cresol with a concomitant increase in 2,6-xyelenol concentration in the product for the feeds with high methanol content further supports our observation that consecutive alkylations occur on these catalysts.

The activity and 2,6-xylenol selectivity over these catalysts may be explained by invoking acid–base and structural properties. Metal oxides are known for their acid–base properties; the respective strengths and acidity-to-basicity ratios depend on its composition. The TPD of NH_3 and CO_2 would be expected to shed light on the acid–base properties of $Cu_xMn_{3-x}O_4$ oxide catalysts that can be correlated with catalytic activity in phenol methylation. Phenol methylation is known to be catalyzed by proton acceptor (basic) sites present on Mn_3O_4 [10]. TPD of CO_2 on $CM_{0.25}$ showed that the sample had relatively high basicity compared with pure manganese oxide. Addition of a small fraction of copper ($x = 0.25$) helped generate relatively high basicity [28,29]. In addition, all of the samples had acidity, as observed from TPD of NH_3 (Fig. 9b). Selectivity to 2,6-xylenol increased with the addition of copper into the hausmannite Mn_3O_4 structure. At the same time, the total acidity,

derived from TPD of NH_3, increased with increasing copper content. The high-copper content samples did not demonstrate desorption of ammonia at higher temperatures, indicating the absence of relatively strong acidity. Hence, we presume that high basicity along with matching acidity were responsible for high 2,6-xylenol selectivity.

Powder XRD showed that the CM_0, $CM_{0.25}$, and $CM_{0.5}$ samples had a hausmannite structure, whereas the other two samples were crystallized as $Cu_{1.5}Mn_{1.5}O_4$ phases. This clearly shows that structural changes occurred on subsequent addition of copper to hausmannite spinel. Considering the initial stages (TOS = 1 h) of the reaction, catalysts with $Cu_{1.5}Mn_{1.5}O_4$ phase ($CM_{0.75}$ and $CM_{1.0}$) seemed to be good; however, they deactivated rapidly after 1 h TOS (Fig. 1). The high concentration of copper in the sample may have promoted its easy reduction, possibly leading to a loss of catalytic activity over these catalysts. Higher copper content also may have shifted the red–ox equilibrium $Cu^{2+} + Mn^{3+} \rightleftarrows Cu^{1+} + Mn^{4+}$ to the right, possibly facilitating easy reduction of copper cations to copper metal. The above interpretation is fully supported by our XPS results.

Catalyst $CM_{0.25}$ showed higher activity and selectivity continuing for up to 5 h TOS compared with the other catalysts. The rapid deactivation of catalysts with high copper content may be attributed to phase changes occurring during the course of the reaction, leading to the formation of MnO and metallic copper; however, deactivation (at least in the initial stages) as a result of carbonaceous deposits cannot be ruled out. All of these results demonstrate that on-stream stability is low for oxide phases that are rich in copper, such as the $Cu_{1.5}Mn_{1.5}O_4$ phase.

XRD of spent catalysts showed the presence of MnO, which has lower-valent manganese than the average valence of Mn in a typical hausmannite phase. Similarly, peaks belonging to Cu metal could be clearly seen in all of the samples with higher Cu content ($x \geqslant 0.5$), whereas hardly any metallic Cu could be seen in the case of $x = 0.25$, although the presence of MnO was detected. However, the hausmannite phase was not retained for this sample, and this sample likely contained well-dispersed metallic copper in addition to MnO. Very low Cu content on the spent $CM_{0.25}$ catalyst from XPS indeed indicates that the amount of Cu on the surface was much lower than that on the corresponding fresh catalyst. However, the high Mn content on spent $CM_{0.25}$ supports the distribution of Cu throughout the catalyst due to reaction-induced structural changes. Compared with other compositions, the $CM_{0.25}$ catalyst may have retained hausmannite structure for a little longer on stream, delaying its deactivation. The control experiment of phenol methylation on MnO under identical conditions showed no activity. Decomposition of methanol on $CM_{0.25}$ under methylation conditions produced CO, CO_2, and H_2. This finding, along with our earlier observation that the sample was reduced to metallic copper and MnO after TPR experiments, proves that reduction of catalysts occurred at high reaction temperatures (673 K), leading to the formation of MnO and Cu, which are not active for phenol methylation. Adding water to the feed did not improve the catalyst life, in contrast to the findings of Thomas et al. over Cu–Co ferro spinels [27]. Hence, it may be concluded that present catalysts are prone to irreversible deactivation under the reaction conditions.

The change in the electronic spectra of the catalysts with varying copper content can be explained based on the red–ox reaction. With increasing copper concentration, Cu^{2+}/Cu^{1+} would be expected to replace Mn^{2+} in the hausmannite lattice. Cu^{1+} shows no d–d transitions, because it is a d^{10} system. A shift in the absorption band in the UV region to lower wavelengths is attributed to the incorporation of Cu^{2+}/Cu^{1+} in place of Mn^{2+}. This band in the UV region for catalysts with $x \geqslant 0.5$ can be assigned to either an $O^{2-} \rightarrow Cu^{2+}$ or an $O^{2-} \rightarrow Mn^{2+}$ charge transfer. The reduced intensity of the visible region band on incorporation of higher amounts of copper ($x \geqslant 0.5$) might be due to a change in the oxidation state from Mn^{3+} to Mn^{4+}. Because no absorption was seen in the visible region at 800 nm, the possibility of Cu^{2+} in octahedral environment clearly can be ruled out. At low concentration, copper may simply replace Mn^{2+} in the tetrahedral sites, because no absorption bands due to Cu^{2+} in octahedral sites were observed. FTIR spectra corroborate the UV results; the structural vibrations observed for CM_0 and $CM_{0.25}$ were in good agreement with the hausmannite structure [43,46,47]. Further increases in copper content led to the transformation of hausmannite to the $Cu_{1.5}Mn_{1.5}O_4$ phase; as a result, the IR bands at 623 and 516 cm^{-1} disappeared from these samples.

It is easier to assign various reduction peaks in a TPR profile obtained for single-oxide systems; however, it is difficult to interpret the TPR profiles of the present system, because they contain various combinations of oxidation states of copper and manganese. Hence, it is not possible to attribute individual peaks to defined red–ox species. As mentioned earlier, the low-temperature TPR peak at 445 K is due to the reduction of Mn^{4+} ions formed as a result of red–ox equilibrium between $Cu^{2+} + Mn^{3+}$ and $Cu^{1+} + Mn^{4+}$ pairs. The increased intensity of the low-temperature peak with copper content further supports this interpretation. Previous reports suggest that copper is reduced at higher temperatures in mixed oxides compared with CuO [37,60]. Hence, the low-temperature peak, the intensity of which increases with increasing copper content, might be due to a shift in equilibrium leading to more Mn^{4+} species. A low-temperature shift of the most intense peak as a result of copper substitution in the manganese oxide spinel has been reported [37,60]. Cu^{2+} may reduce to metallic Cu either in a single step or in two steps, that is, $Cu^{2+} \rightarrow Cu^{1+} \rightarrow Cu^0$. On the other hand, reduction of Cu^{2+} in pure CuO occurs at 523 K, as reported by Tanaka et al. [61]. The observation of a single reduction peak for this system may be attributed to the formation of copper–manganese oxide solid solution as a result of $Cu^{2+/1+}$–O–Mn^{3+}/Mn^{4+} bonds. These results are in good agreement with those reported for such spinels [61].

The splitting of Mn 2p and the Mn 3s is often used to determine the manganese oxidation states [50]. Mn 2p shake up satellites also may be expected, because all 3d configurations of manganese are paramagnetic [62]. But the satellites are clearly observed only for MnO. For Mn_2O_3 and MnO_2, Mn $2p_{1/2}$ peaks are superimposed on the satellites [62]. The BE value of 642.0 eV for CM_0 sample may be attributed to Mn_3O_4 phase,

which supports powder XRD results. The Mn $2p_{3/2}$ BE of pure Mn_3O_4 is expected to be between the BE values of Mn^{3+} and Mn^{2+}; however, the impurity present in the catalysts (i.e., Mn_5O_8, with average oxidation state of +3.2) might shift these BEs higher. Incorporation of copper (Cu^{+}) into tetrahedral sites of hausmannite is expected to shift the BE of Mn 2p higher due to the formation of Mn^{4+} ($Cu^{2+} + Mn^{3+} \rightleftarrows Cu^{1+} + Mn^{4+}$). These observations are in good agreement with previous reports [54]. The BE of spent catalyst at ⩽641.4 eV is attributed to the presence of Mn^{2+}, although some amount of Mn^{3+} cannot be ruled out. The formation of MnO after phenol methylation was also confirmed with XRD. The ratio of Cu to Mn on the surface was estimated as reported previously [27]. The integrated intensities of the Cu 2p and Mn 2p peaks have been taken into account to estimate the concentration. The surface copper was enriched 1.3-fold on $CM_{0.25}$, whereas the bulk and surface compositions were nearly same on $CM_{1.0}$.

Although the BE of Cu $2p_{3/2}$ from spent catalysts was close to Cu^{1+}, we presume that it was copper metal, based on the powder XRD results. Cation distribution is generally deciphered based on XPS results. Thermodynamic calculations for site preference energy of several bivalent and trivalent cations in spinel structures [63] showed higher octahedral site preference energy for Mn^{3+}/Mn^{4+} than for Cu^{2+}. On the other hand, Mn^{2+} and Cu^{1+} both have a greater preference for tetrahedral sites. However, some reports suggest presence of bivalent copper, at least a part of it, in octahedral sites [63]. For copper-containing spinels, most reports agree with the location of monovalent copper in tetrahedral and bivalent copper in octahedral sites [64]. The literature reports that the BE values of the copper Cu $2p_{3/2}$ peak in spinels follow the order $Cu^{+}(O_h) < Cu^{+}(T_d) < Cu^{2+}(O_h) < Cu^{2+}(T_d)$ [65].

4.1. Relationship between catalytic activity and acid–base property

Previous reports on the correlation of acid–base properties to catalytic methylation of phenol to yield various methyl phenols were not helpful in comparing or generalizing our catalytic oxide system. Hence, we speculate on a possible correlation based on our phenol methylation reaction results. The performance of $CM_{0.25}$ showed that it had higher activity and also better selectivity toward 2,6-xylenol yield. In general, the Lewis acidity can be attributed to the metal ions, whereas the basicity can be attributed to the presence of oxide anions on the surface of a metal oxide. Obviously, the catalyst's compositional variation influences the distribution of metal and oxide ions, as well as their strengths. It is known that Mn_3O_4 is a basic oxide, and that adding copper should further enhance the basicity of the system. But the surface acid–base property of the oxide catalysts strongly depends on the nature and content of surface cations. Many reports claim that acidity is the determining factor in phenol conversion activity, whereas basicity accounts for 2,6-xylenol selectivity. The better activity and selectivity on $CM_{0.25}$ may be attributed to the presence of Cu^{2+}, which might account for the better 2,6-xylenol selectivity as well as greater structural stability. According to Thomas et al., Cu^{2+} is the active species, and its synergetic interaction with other metal cations (Co) present in the system leads to better 2,6-xylenol selectivity [27].

4.2. Electronic and structural changes

The changes occurring in the electronic properties of the catalysts during the reaction can be explained by our XRD, TPR, and XPS findings. A reducing atmosphere was created during the phenol methylation reaction, confirmed by the observation of H_2 and CO, probably formed by steam reforming/decomposition of methanol. These reducing gases (H_2 and CO) were responsible for the catalyst reduction, resulting in the formation of Cu and MnO. These reduced species were not active for phenol methylation, and hence the catalysts deactivated after a few hours. This reduction is confirmed by XRD of spent catalysts, which exhibited Cu metal and MnO. XPS findings also corroborate the above observations. The changes observed on main peaks, satellites, and Auger features of Mn and Cu provide clearly indicate that partial reduction of these species occurred during the reaction. It is useful to highlight the following features from XPS:

1. Copper reduction was seen for $x > 0.25$, with the extent of reduction increasing linearly with increasing "x" value.
2. Partial reduction of all metal ions and a consequent increase in the energy overlap of 3d band in the spent catalysts occurred.
3. A comparable activity was observed for $x = 0$–0.5, indicating the equal importance of Cu^{2+} and Mn^{3+} for better performance.
4. The complete phase change of the catalysts after reaction, identified on XRD and XPS, hints at the structural collapse.

All of the above points indicate considerable redistribution of the cations under reaction conditions.

The extent of red–ox interaction between Mn^{3+} and Cu^{2+} increased with increasing x value. This is confirmed by the formation of $Cu_{1.5}Mn_{1.5}O_4$ phase seen on XRD. The extent of reduction in $CM_{1.0}$ reached 45% (reducibility of Cu, calculated as the amount of reduced Cu to Cu^{2+}content). The activity and selectivity were higher on $CM_{0.25}$, because the extent of reduction was minimum (as confirmed by XRD and XPS). Although the overlap of 3d bands from Cu and Mn in the fresh catalysts would be expected to enhance activity and selectivity through synergetic interaction [27], the increased reduction with higher copper content led to poor activity and selectivity. But the better overlap of 3d bands could not be used in phenol methylation due to reductive atmosphere (structure collapse) and high extent of reduction. However, these processes are relatively low in $CM_{0.25}$, contributing to the higher activity for phenol methylation and 2,6-xylenol selectivity.

4.3. Mechanism of C-methylation of phenol

Two pathways are proposed for the formation of 2,6-xylenol by the methylation of phenol. One probable path is through the

formation of anisole, which further reacts with methanol to give 2,6-xylenol via isomerization of methyl anisole. The alternate route is through the C-alkylation of phenol to give *o*-cresol, followed by its consecutive methylation to give 2,6-xylenol. In either case, the first key step in the methylation of phenol is the adsorption of phenol on the catalyst surface. Tanabe et al. [9] supported the second mechanism, wherein C-alkyl phenols are formed through the adsorption of phenolate ion, in a perpendicular orientation, on an MgO catalyst system. This particular orientation of the phenolate ion on the catalyst surface leads to its methylation in the ortho position. Because we did not observe anisole under any of our reaction conditions, we feel that the latter mechanism proposed by Tanabe et al. may be the most probable and applicable to our catalytic system. The enhanced 2,6-xylenol selectivity at the expense of *o*-cresol and further methylation of 2,6-xylenol, leading to trimethyl phenol (mesitol), demonstrates that the reaction is consecutive, giving further credence to the above mechanism.

5. Conclusion

A series of copper manganite spinel catalysts ($Cu_xMn_{3-x}O_4$, $x = 0$–1) were prepared and used for phenol methylation. The initial activity of these catalysts increased with increasing copper content. Higher copper-containing catalysts were found to be more prone for reduction under reaction conditions, leading to rapid deactivation. The catalyst with low copper content ($CM_{0.25}$) was more active and selective for 2,6-xylenol. All of the catalysts, irrespective of their composition, produced only C-methylated phenols. XRD, UV–vis, and FTIR results revealed that CM_0 and $CM_{0.25}$ had a hausmannite phase that underwent minimal reduction in reaction conditions and that $CM_{0.25}$ was relatively stable for phenol methylation compared with the other catalysts studied. In contrast, $CM_{0.75}$ and $CM_{1.0}$, which exhibited $Cu_{1.5}Mn_{1.5}O_4$ oxide phase, showed good initial activity but deactivated rapidly. The strong basicity and weak acidity associated with these catalysts were responsible for the selective formation of 2,6-xylenol. Among the catalysts studied, $CM_{0.25}$ was found to have optimum acid–base properties.

Acknowledgments

A.S.N.R. thanks the University Grants Commission (UGC) for a research fellowship. The authors thank Dr. S.P. Mirajkar and Ms. Violet Samuel for their help in obtaining the TPD, TPR, and XRD measurements.

References

[1] H. Fiege, Ullman's Encyclopedia of Industrial Chemistry, vol. A8, fifth ed., VCH, Weinheim, 1987, p. 25.
[2] K. Weissermel, H.J. Arpe, Industrial Organic Chemistry, Verlag Chemie, Weinheim, 1978, p. 316.
[3] B.L. Leach, U.S. patent 3994982, 1976.
[4] M. Kawamata, K. Ohshima, A. Kudoh, M. Kotani, U.S. patent 4208537, 1980.
[5] K. Tanabe, T. Nishizaki, in: F.C. Tompkins (Eds.) Proceedings of the Sixth International Congress on Catalysis, vol. 2, London, 1977, p. 863.
[6] S. Velu, C.S. Swamy, Appl. Catal. A Gen. 145 (1996) 141.
[7] W.C. Choi, J.S. Kim, T.H. Lee, S.I. Woo, Catal. Today 63 (2000) 229.
[8] V. Venkat Rao, V. Durga Kumari, S. Narayanan, Appl. Catal. 49 (1989) 165.
[9] K. Tanabe, K. Shimadzu, H. Hattori, K. Shimadzu, J. Catal. 57 (1979) 35.
[10] C. Benzouhanova, M.A. Al-Zihari, Appl. Catal. A Gen. 83 (1992) 45.
[11] S. Sato, K. Koizumi, F. Nozaki, Appl. Catal. A Gen. 133 (1995) L7.
[12] T. Kotanigawa, M. Yamamoto, K. Shimokawa, Y. Yoshida, Bull. Chem. Soc. Jpn. 44 (1971) 1961.
[13] T.F. Tsai, F.L. Wang, Catal. Lett. 73 (2–4) (2001) 167.
[14] T.M. Jyothi, S. Sugunan, K. Sreekumar, M.B. Talawar, B.S. Rao, Ind. J. Chem. Tech. 7 (2000) 155.
[15] K. Tanabe, H. Hattori, T. Sumiyoshi, K. Tamaru, T. Kondo, J. Catal. 53 (1978) 1.
[16] S. Sato, K. Koizumi, F. Nozaki, J. Catal. 178 (1998) 264.
[17] S. Sato, R. Takahashi, T. Sodesawa, K. Matsumoto, Y. Kamimura, J. Catal. 184 (1999) 180.
[18] M.C. Samolada, E. Grigoriadou, Z. Kiparissides, I.A. Vasalos, J. Catal. 152 (1995) 52.
[19] S. Velu, C.S. Swamy, Appl. Catal. A Gen. 119 (1994) 241.
[20] P. Beltrame, P.L. Beltrame, P. Carniti, A. Castelli, L. Forni, Appl. Catal. 29 (1987) 327.
[21] E. Santacesaria, M. Diserio, P. Ciambelli, D. Gelosa, S. Carra, Appl. Catal. 64 (1990) 101.
[22] S. Balsama, P. Beltrame, P.L. Beltrame, P. Carniti, L. Forni, G. Zuretti, Appl. Catal. 13 (1984) 161.
[23] E. Santacesaria, D. Grasso, D. Gelosa, S. Carra, Appl. Catal. 64 (1990) 83.
[24] G.D. Yadav, Parveen Kumar, Appl. Catal. A Gen. 286 (2005) 61.
[25] K. Tanabe, in: B. Imelik, C. Naccache, G. Coudurier, Y.B. Taarit, J.C. Vedrine (Eds.), Stud. Surf. Sci. Catal., vol. 20, Elsevier, Amsterdam, 1985, chap. 1.
[26] K. Sreekumar, S. Sugunan, J. Mol. Catal. A Chem. 185 (2002) 259.
[27] T. Mathew, N.R. Shiju, K. Sreekumar, B.S. Rao, C.S. Gopinath, J. Catal. 210 (2002) 405.
[28] T. Mathew, B.B. Tope, N.R. Shiju, S.G. Hegde, B.S. Rao, C.S. Gopinath, Phys. Chem. Chem. Phys. 4 (2002) 4260.
[29] T. Mathew, M. Vijayaraj, S. Pai, B.B. Tope, S.G. Hegde, B.S. Rao, C.S. Gopinath, J. Catal. 227 (2004) 175.
[30] K. Sreekumar, T. Mathew, R. Rajagopal, R. Vetrivel, B.S. Rao, Catal. Lett. 65 (2000) 99.
[31] K. Sreekumar, T. Mathew, B.M. Devassy, R. Rajgopal, R. Vetrivel, B.S. Rao, Appl. Catal. A Gen. 205 (2001) 11.
[32] K. Sreekumar, T.M. Jyothi, T. Mathew, M.B. Talwar, S. Sugunan, B.S. Rao, J. Mol. Catal. A Chem. 159 (2000) 327.
[33] R. Dowbenko, in: J.I. Kroschwitz, M. Howe-Grant (Eds.), Kirk-Othmer Encyclopedia of Chemical Technology, vol. 2, fourth ed., 1999, p. 106.
[34] G.C. Chinchen, K.C. Waugh, D.A. Whan, Appl. Catal. 25 (1986) 101.
[35] L.S. Puckhaber, H. Cheung, D.L. Cocke, A. Clearfield, Solid State Ionics 32–33 (1989) 206.
[36] S. Veprek, D.L. Cocke, S. Kehl, H.R. Ostwald, J. Catal. 100 (1986) 250.
[37] A. Wöllner, F. Lange, H. Schmelz, H. Knözinger, Appl. Catal. A 94 (1993) 181.
[38] J.G. Christian, J.E. Johnson, Int. J. Air Wat. Poll. 9 (1965) 1.
[39] J.K. Musick, F.W. Williams, Ind. Eng. Chem. Prod. Res. Dev. 13 (1974) 175.
[40] R.W. McCabe, P.J. Mitchell, Ind. Eng. Chem. Prod. Res. Dev. 23 (1984) 196.
[41] S.B. Kanungo, J. Catal. 58 (1979) 419.
[42] N.F.M. Henry, H. Lipson, W.A. Wooster, The Interpretation of X-Ray Diffraction Photographs, Macmillan, London, 1951.
[43] V.S. Escribano, E.F. López, P.S. Huidobro, M. Panizza, C. Resini, J.M. Gallardo-Amores, G. Busca, Solid State Sci. 5 (2003) 1481.
[44] D.M. Sherman, N. Vergo, Am. Miner. 73 (1988) 140.
[45] W.S. Kijlstra, E.K. Poels, A. Bliek, B.M. Weckhuysen, R.A. Schoonheydt, J. Phys. Chem. B 101 (1997) 309.
[46] J.M. Gallardo-Amores, T. Armaroli, G. Ramis, E. Finocchio, G. Busca, Appl. Catal. B Environ. 22 (1999) 249.
[47] F. Milella, J.M. Gallardo-Amores, M. Baldi, G. Busca, J. Mater. Chem. 8 (11) (1998) 2525.

[48] S. Velu, K. Suzuki, M. Okazaki, M.P. Kapoor, T. Osaki, F. Ohashi, J. Catal. 194 (2000) 373.
[49] P. Porta, M.C. Campa, G. Fierro, M. Lo Jacono, G. Minelli, G. Moretti, L. Stoppa, J. Mater. Chem. 3 (5) (1993) 505.
[50] S.M. Rodulfo-Baechler, S.L. González-Cortés, J. Orozco, V. Sagredo, B. Fontal, A.J. Mora, G. Delgado, Mater. Lett. 58 (2004) 2447.
[51] V. Koleva, D. Stoilova, D. Mehandjiev, J. Solid State Chem. 133 (1997) 416.
[52] G. Fierro, S. Morpurgo, M. Lo Jacono, M. Inversi, I. Pettiti, Appl. Catal. A Gen. 166 (1998) 407.
[53] C.D. Wagner, W.M. Riggs, L.E. Davis, J.F. Moulder, Handbook of Photoelectron Spectroscopy, Perkin–Elmer Corp. Physical Electronics Div., Eden Prairie, MN, 1979.
[54] N.S. McIntyre, M.G. Cook, Anal. Chem. 47 (1975) 2208.
[55] M. Oku, K. Hirokawa, S. Ikeda, J. Electron Spectrosc. Relat. Phenomen. 7 (1975) 465.
[56] G.C. Allen, S.J. Harris, J.A. Jutson, J.M. Dyke, Appl. Surf. Sci. 37 (1989) 111.
[57] S. Angelov, E. Zhecheva, K. Petrov, D. Mehandjiev, Mat. Res. Bull. 17 (1982) 235.
[58] B.L. Yang, S.F. Chan, W.S. Chang, Y.Z. Chen, J. Catal. 130 (1991) 52.
[59] J.J. Yeh, I. Lindau, At. Data Nucl. Data Tables 32 (1985) 1.
[60] M. Vijayraj, C.S. Gopinath, J. Catal. 241 (2006) 83.
[61] Y. Tanaka, T. Utaka, R. Kikuchi, T. Takeguchi, K. Sasaki, K. Eguchi, J. Catal. 215 (2003) 271.
[62] L. Yin, I. Adler, T. Tsang, L.J. Matienzo, S.O. Grim, Chem. Phys. Lett. 24 (1974) 81.
[63] A. Navrotsky, O.J. Kleppa, J. Inorg. Nucl. Chem. 29 (1967) 2701.
[64] J. Töpfer, A. Feltz, P. Dordor, J.P. Doumerc, Mat. Res. Bull. 29 (1994) 225.
[65] C. Drouet, C. Laberty, J.L.G. Fierro, P. Alphonse, A. Rousset, Int. J. Inorg. Mater. 2 (2000) 419.